Microscopy Techniques

4

Antonia Feola, Letizia Cito, Angelina Di Carlo, Alfonso Giovane, and Marina Di Domenico

Phase Contrast

Phase contrast microscopy is a contrast-enhancing optical technique that can be applied to unstained biological specimens because it improves the contrast images of transparent specimens without affecting resolution. It is mainly used to examine dynamic events in living cells [1–7].

Two parameters should be considered in phase contrast microscopy: the light wave amplitude and the light wave phase. Changes in amplitude are due to the absorption or scattering of light. The human eye is only sensitive to amplitude variations that are perceived as changes in brightness and cannot perceive changes in phase. The technique is based on an optical mechanism that converts light phase variations to changes in amplitude, which can be visualized as differences in image contrast. To make phase changes visible in phase contrast microscopy, the illuminating light background is separated from the specimen's scattered light. In a normal microscope, the illumination of an unstained biological specimen produces a weak scattered light, the phase of which is usually shifted by 90°, resulting in a low-contrast image. In the phase contrast microscope, the phase of background light is shifted by 90° by passing it through a phase shift ring. Thus, the phase difference between the background and the scattered light is eliminated, producing an increased contrast. One of the advantages of phase contrast microscopy is that living cells can be examined in their natural state without killing, fixing, and staining them [8–10]. This technique enables the observation and recording of biological processes in high contrast with sharp clarity [11–14]. Prior to the invention of phase contrast techniques, transmitted bright field illumination was one of the most commonly used tools in optical microscopy, especially for fixed stained specimens or other types of samples showing high natural absorption of visible light. The addition of phase contrast optical accessories to a standard bright field microscope can be

A. Feola (✉)
Department of Biology, University of Naples "Federico II", Via Cinthia, 2, 80126 Naples, Italy
e-mail: antonia.feola@unina.it

L. Cito
INT-CROM, "Pascale Foundation" National Cancer Institute-Cancer Research Center, 83013 Mercogliano, Italy
e-mail: letizia.cito@cro-m.eu

A. Di Carlo
Department of Medico Surgical Sciences and Biotechnologies, University of Rome "Sapienza", Corso della Repubblica, 79, 04100 Latina, Italy
e-mail: angelina.dicarlo@uniroma.it

A. Giovane • M. Di Domenico
Department of Biochemistry, Biophysics and General Pathology, Seconda Università degli Studi di Napoli, Via de Crecchio, 7, 80138 Naples, Italy
e-mail: alfonso.giovane@unina2.it; marina.didomenico@unina2.it

F.M. Sacerdoti et al. (eds.), *Advanced Imaging Techniques in Clinical Pathology*, Current Clinical Pathology, DOI 10.1007/978-1-4939-3469-0_4

employed as a technique to render a contrast-enhancing effect in transparent specimens, similar to optical staining. So far, modern phase contrast microscopes enable the detection of specimens with very small internal structures, or even just a few protein molecules, when the technology is coupled to electronic enhancement and post-acquisition image processing [15–17].

Differential Interference Contrast (DIC)

Differential interference contrast (DIC) is a mechanism for enhancing contrast in transparent specimens. It produces contrast by visually showing the refractive index gradients of different areas of a specimen. The invention in 1950 is attributed to Georges Nomarski, who modified the Wollaston prism. The modification consists in cutting one edge of the prism in such a manner that the optical axis is oriented obliquely with respect to the flat surface of the prism. This modification causes the light rays to come to a focal point outside the body of the prism. The light beam is polarized and then split into two separate beams, the distance of which is equal to the resolution of the objective lens. One beam path is directed through the specimen and the other acts as a reference beam; the two beams are then combined. Since different parts of the specimen have different refractive indices, when the beams are gathered by a second polarizing filter, the vibrational planes of the beams is restored; this causes variations in amplitude that are visualized as differences in brightness [18–25].

DIC microscopy has the following advantages:

- It is possible to make fuller use of the numerical aperture of the system.
- There are no confusing halos.
- Images can be seen in striking color (optical staining) and with a 3D shadow-like appearance. The visibility of outlines and details is greatly improved, and the photomicrography of these images is striking in color and detail.
- Regular planachromats or achromats (also suitable for ordinary bright-field work) can be used if the manufacturer states that such objectives are designed for their apparatus.

DIC also has the following disadvantages or limitations:

- The equipment for DIC is quite expensive because of the many prisms that are required.
- Birefringent specimens, such as those found in many kinds of crystals, may not be suitable because of their effect on polarized light. Similarly, specimen carriers, such as culture vessels and Petri dishes made of plastic may not be suitable. For such specimens, Hoffman modulation contrast may be a better choice.
- Apochromatic objectives may not be suitable because such objectives themselves may significantly affect polarized light.
- For very thin or scattered specimens, better images may be achieved using phase contrast methods. DIC microscopy has been used to assess the new bone formation and microstructure [26], to detect retinitis pigmentosa [27], to measure the lamellarity of giant lipid vesicles [28], to quantify volume, mass, and density of thrombus formation [29]. Furthermore, three-dimensional imaging of cell division and analysis of microtubule dynamic were studied by this technique [30, 31].

Wide-Field Fluorescence

Wide-field fluorescence or epi-fluorescence microscopy is a common technique used to acquire both topographical and dynamic information. It is based on the irradiation of the whole sample with a light of a specific wavelength, and the weaker emitted fluorescence is then separated from the stronger excitation light. The microscope is configured in such a way that only the emission light can reach the detector or eye. The resulting fluorescent image is superimposed with high contrast against a black

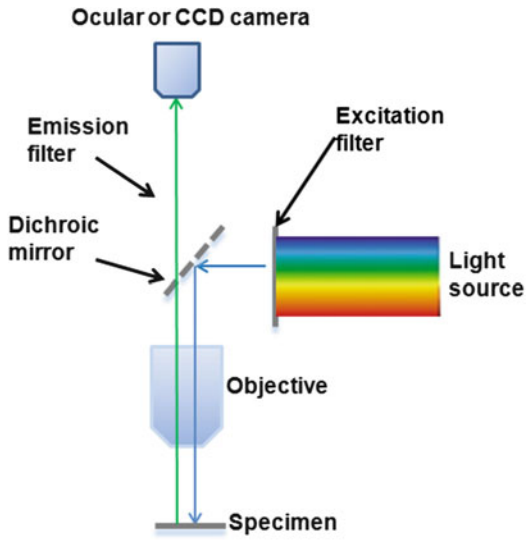

Fig. 4.1 Schematic representation of a wide-field microscope

background. The limits of detection are generally regulated by the contrast between the fluorescent image and the darkness of the background. A fluorescence microscope, as shown in Fig. 4.1, basically constitutes an arc lamp (usually a mercury or xenon), an optical tube containing exciting filters producing a defined band of wavelengths, a dichroic mirror (which has the ability to reflect excitation wavelengths and pass emission wavelengths), and an emission filter (also known as a barrier filter). These three components are the heart of the system and are usually assembled by the manufacturer in a block or cube to give the right monochromatic light beam to produce the best signal-to-noise ratio. The light emerging from the emission filter is then captured by an observation tube that can be connected to an eyepiece or a digital camera. The excitation light is directed onto the specimen by passing it through the selected excitation filter and then through the microscope objective, which acts as a condenser. The light beam reaches the specimen, the emitted fluorescence then passes through the same objective, reaching the ocular or the digital camera. Therefore, both the illumination and the detection of light take place simultaneously and cover the whole visual field, depending on the microscope objective.

Filters play a fundamental role in fluorescence microscopy, with two types generally used: a band-pass filter and a long pass filter. The band-pass filter transmits a light of a discrete wavelength that has a maximum centered in the range of 20–40 nm. The long pass filter cuts off the light lower than a certain wavelength and transmits light higher than that wavelength.

The excitation filter is usually a band-pass filter that passes only light of the right wavelength for fluorophore excitation. The emission or barrier filter is generally a long pass filter and separates fluorescence produced by the fluorophore from background light. The barrier filter transmits light of the fluorescence wavelength coming from the dichroic mirror while blocking all other light from the excitation lamp (reflected from the specimen or optical elements). This is necessary because the intensity of fluorescent light is about 100,000-fold weaker than the excitation light.

The dichroic mirror is a filter and a mirror at the same time because it reflects the light coming from the excitation filter and passes the fluorescent light coming from the specimen. A dichroic mirror used in an epi-fluorescence microscope is placed at 45° with respect to the excitation light, which is reflected 90° toward the objective and the specimen. The fluorescence light coming from the specimen passes through the dichroic mirror, directed toward the observer (or high-sensitivity camera) [32–34].

Fluorescence is usually used to increase the sensitivity of different techniques. When a light beam of a certain energy $E_i = h\nu_i$ interacts with a fluorescent molecule, it can be absorbed if its energy is equal to or greater than the energy necessary to promote a quantum leap of an electron belonging to that molecule. The electron in the excited state decays to the ground state by emitting a radiative energy $E_{em} = h\nu_{em}$ were h is the Planck constant and ν is the frequency. Since most fluorophores have a larger dipole moment in the excited state than in the ground state, the solvent molecules can reorient around the excited molecule, lowering its energy. Thus, E_{em} becomes lesser than E_i and $\nu_{em} < \nu_i$ but frequency is inversely proportional to wavelength according to the equation $c = \nu\lambda$ (where

c is the light velocity). Thus, the emission light has a longer wavelength of exciting light; this phenomenon is known as Stokes shift. The dimension of the shift depends on the molecular structure, which ranges from a few nanometers to several hundred nanometers. Generally, fluorophores used in microscopy range between 20 and 100 nm. The occurrence of Stokes shift is critical to an increase in sensitivity of fluorescence imaging measurements. The emission shift allows the use of optical filters with a bandwidth that efficiently blocks excitation light from reaching the detector; therefore, the relatively low fluorescence signal can be observed with a low-noise background.

In addition to the Stokes shift, other parameters are important in defining fluorophores, as follows:

The extinction coefficient (ε)
The fluorescence lifetime (τ)
The quantum yield (Φ)

The molar extinction coefficient ε is defined as the absorption produced by a 1 M solution of a substance at a particular wavelength (usually that of maximum absorption), determined in a cuvette of 1 cm path length. Extinction coefficient is a direct measure of the ability of a molecule to absorb light; fluorophores with a high extinction coefficient also have a high probability of high fluorescence emission.

The fluorescence lifetime τ is the time that a molecule remains in an excited state prior to returning to the ground state. Because the lifetime of a fluorophore is inversely proportional to the extinction coefficient, molecules with a high extinction coefficient have an excited state with a short lifetime. Fluorescence intensity is proportional to the number of molecules in the excited state; however, in the excited state, a molecule possesses a dipolar moment that can be perturbed by several factors such as solvent polarity, collision with other molecules in the ground state, temperature, and pH. These factors contribute to the relaxation of the excited state dispersing its energy in a non-radiative form, thus decreasing fluorescence intensity (this decrease is called fluorescence quenching). The parameter that describes the fluorescence intensity is the quantum yield Φ, which is the ratio between the photons emitted and the photons absorbed. As calculated, this parameter has a dimensionless value ranging between 0 and 1; however, the value almost never reaches 1. Quantum yield is the fluorescence equivalent of the molar extinction; fluorophores with high quantum yield produce a more intense signal, thus increasing the measure sensitivity. However, care should be taken in measuring the fluorescence intensity of probes in living cells because it may change according to the cellular district because of differing pH or polarity. Photobleaching is another event that affects fluorescence. This phenomenon, while not yet completely understood, is responsible for a decrease in fluorescence from a long irradiation of molecules and seems to be due to the interaction of oxygen with the excited fluorophore. In fact, the oxygen dissolved in the sample medium can interact in its triplet ground state with a particular excited state of the fluorophore in which a cross from singlet to triplet status occurs. Since the molecule in the triplet state has a lifetime of a millisecond—versus the nanosecond in singlet state—it can interact with oxygen for longer, generating an oxygen radical. The oxygen radical reacts with the more reactive fluorophore in its excited state, thus quenching the fluorescence [35].

Fluorescence microscopy is now one of the most used techniques in biology, thanks to the availability of a large number of fluorophores (also named dyes) synthesized to respond to several characteristics such as high quantum yield, large Stokes shift, and resistance to photobleaching.

Dyes can be modified to bind to specific biological targets. A dye modified in this manner is called a probe. Several probes are synthesized to monitor the most diverse biological functions in living cells, such as chelation to ions, pH sensitivity, and lipid transport and metabolism [36–42]. Furthermore, a dye can be linked to an antibody to study a localization of a specific protein in a fixed cell or tissue [43]. Moreover, fluorescence microscopy can also be used for DNA imaging [44, 45]. However, if different probes are used simultaneously, several target

molecules can be identified in the same specimen.

Confocal Microscopy

Confocal microscopy has significant advantages over wide-field microscopy. In particular, it can produce images with reduced degradation as most of the out-of-focus light from the specimen is removed [46]. Furthermore, this technique enables the acquisition of a series of optical sections along the thickness of the specimen (z axis). In a wide-field fluorescence microscope, the fluorescence emitted by the specimen comes from that emitted not only by the focal plane but also by the layers up and down it, producing an out-of-focus fluorescent light that decreases the image resolution.

Basically, wide-field and confocal microscopes have the same optical light path; however, several differences are encountered along this light path. First, the light beam is generated by a laser source that produces a coherent beam with a greater intensity and a reduced bandwidth. The term "laser" is an acronym of "*l*ight *a*mplification by *s*timulated *e*mission of *r*adiation." Laser light is different from other light sources by virtue of its coherence, which allows the laser beam to be focused to a tight spot, and the narrow beam has limited diffraction. The light beam, like the wide-field microscope, is reflected by a dichroic mirror and passes through the objective, to focus on a very small region of the specimen. The fluorescence emitted by the irradiated point on the specimen passes through the dichroic mirror and reaches the pinhole located just before the emission filter and the detector. This alignment allows the pinhole and the irradiated surface of the specimen to be on the same focal plane (confocal). Thus, only the fluorescence emitted from the specimen surface in the confocal plane can pass through the pinhole, whereas fluorescent light from the specimen regions other than the focal plane is excluded. Moreover, in wide-field fluorescence microscopy, the whole specimen is subject to irradiation of an incoherent light, and the image produced by fluorescence emission can be directly observed in the eyepiece or acquired by a charge-coupled device (CCD) camera. In a confocal fluorescence microscope, the image is produced by scanning the specimen surface with a laser beam and simultaneously acquiring the fluorescent light emission through a photomultiplier so the fluorescence intensity coming from each point scanned is registered by a computer and the whole image is reconstituted via dedicated software. For this purpose, the confocal microscope is equipped with a scan head with optical and electronic components. In fact, the scan head moves the laser beam along the xy axes of the specimen, collects the corresponding fluorescence emission, and sends it to the photomultiplier. When a new specimen region along the z axis is focused, the new region becomes confocal to the observed region on the detector. Thus, images of different specimen slices along the z axis can be obtained and a 3D image can be reconstituted using appropriate software [47, 48].

With respect to the wide-field microscope, excitation and fluorescence intensity can be regulated in several ways in the confocal microscope. In fact, varying the laser energy can regulate the exciting light intensity; fluorescence intensity can be controlled by changing the pinhole diameter and by the photomultiplier gain. Generally, a measurement is a compromise between resolution and sensitivity; this is also true for confocal microscopy. In fact, to increase resolution, the pinhole diameter must be very narrow. Whereas, on one hand, a narrow aperture allows fewer out-of-focus photons to reach the photomultiplier, it also reduces the number of confocal photons reaching the detector, decreasing fluorescence intensity and therefore sensitivity. However, fluorescence intensity can be increased in two ways: by increasing the laser energy or the photomultiplier gain. In the first case, increasing the laser energy produces two negative effects: it increases autofluorescence and photobleaching. In the second case, the increase in gain also increases the background currents of the photomultiplier, thus reducing the signal-to-noise ratio, which affects resolution. Therefore, if only a qualitative determination is required, all these effects hardly affect the measure. However, if a quantitative measurement is

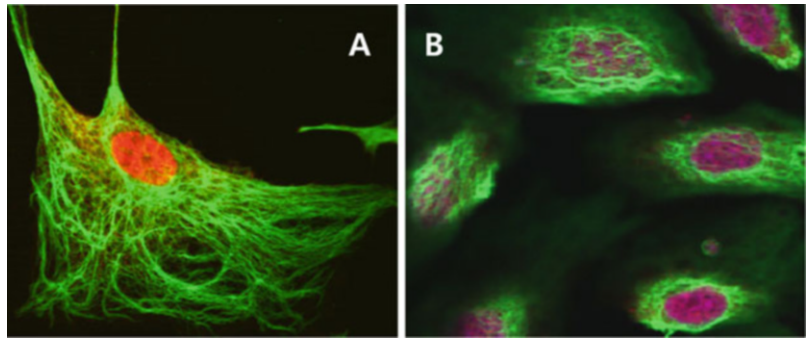

Fig. 4.2 Dual (**a**) and triple (**b**) staining confocal imaging of endothelial cells. (**a**) Vimentin (*green*) and the nuclear protein P16 (*red*) were stained. (**b**) Same as (**a**) but nuclei are stained with DAPI (*blue*). Cell images were acquired via oil-immersed objective (63×), but image (**a**) was further magnified via digital zoom

needed, care should be taken when measuring the fluorescence intensity of the control and the sample with the same microscope settings [49]. Figure 4.2 shows two images of endothelial cells acquired by a confocal microscope stained with double or triple color.

Balestrieri et al. [50] investigated the expression of platelet-activating factor (PAF) receptors in endothelial progenitor cells (EPCs). They demonstrated the presence of PAF receptors by monitoring a transient increase of cytoplasmic Ca^{2+} upon PAF stimulation. The Ca^{2+} transient increase was assessed via laser scanning confocal microscopy in a time-lapse acquisition mode using Fluo 4-AM, a probe that increases its fluorescence when chelated by calcium ions (Fig. 4.3). Confocal microscopy was found useful in elucidating cell organization [51, 52] as well as the molecular mechanisms of neoplastic processes [53–60].

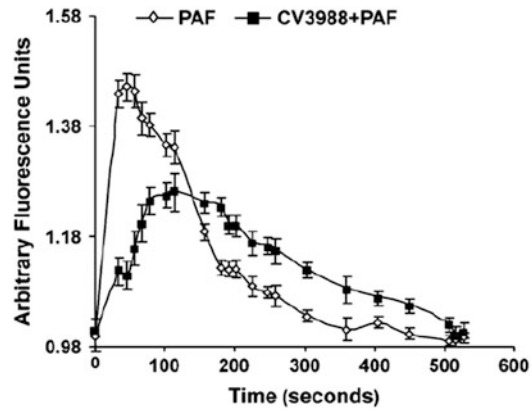

Fig. 4.3 Increase of intracellular Ca^{2+} levels induced by platelet-activating factor (PAF) in the presence and absence of CV3988, a PAF antagonist. Confocal imaging of cells loaded with fluorescent Fluo 4-AM was undertaken using a Zeiss LSM510 system equipped with a 20× (NA) objective. Ca^{2+} ion was measured in time drive configuration (488 nm excitation, 530 nm emission LP510 nm) for 50 slices (about 600 s). In each slice, the fluorescence intensity average was measured by ImageJ free software (http://imagej.nih.gov/ij/)

Total Internal Reflection Fluorescence Microscopy (TIRFM)

Total internal reflection fluorescence microscopy (TIRFM) is based on an optical effect produced by passing a light beam at a high incident angle through glass (i.e., a coverslip) or plastic (i.e., a Petri dish) [61]. The difference in refractive indexes between the glass and the water determines the amount of refraction or reflection light at the interface as a function of beam incident angle. At a specific angle of the glass (or plastic)–water interface, the light beam is totally reflected according to a phenomenon described by Snell that can be summarized by the following equation:

$$n_1 \sin\theta_1 = n_2 \sin\theta_2$$

where n_1 is the medium with the higher refractive index (1.518 for glass microscope slide or coverslip) and n_2 is the medium of the lower refractive index (1.33–1.37 for aqueous buffers). When a light beam impacts upon a medium with an angle θ_1 with respect to the normal, it is refracted with

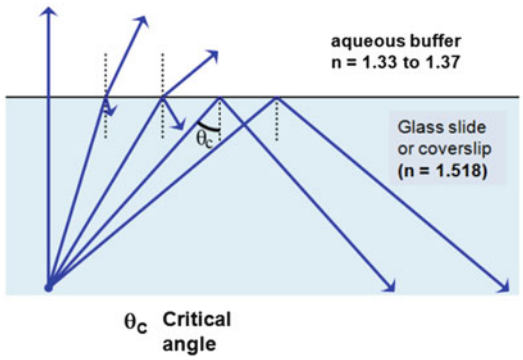

Fig. 4.4 Schematic representation of a light beam reaching the critical angle

an angle θ_2 at the interface into the medium of the lesser refractive index. As the angle θ_1 increases, the beam reaches the critical angle where the refraction is 90°; when the light beam exceeds the critical angle, it is completely reflected at the interface, giving the total internal reflection (Fig. 4.4).

The light reflected generates an electromagnetic field with the same frequency as the incident light; this is called the evanescent wave [62, 63]. Since this wave is produced by a very small (about 200 nm) electromagnetic field and its intensity decreases exponentially with distance, only fluorophores located near the glass–liquid interface can be excited [64, 65]. Thus, fluorophores not in the primary focal plane are not excited; consequently, unwanted secondary fluorescence emission is markedly reduced. This effect produces high-contrast images of the specimen surface with a considerable increase in signal-to-background ratio compared with classical wide-field microscopy [66]. Figure 4.5 is a schematic picture of a TIRF microscope.

In theory, the excitation light could be produced by an arc lamp, but directing the light beam to an appropriate angle while maintaining a suitable intensity is difficult, so a coherent light produced by a laser source is more useful. To obtain a high angle of incidence, the laser irradiates the specimen through the objective lens from the periphery of the back focal plane. The light passes through the objective immersion oil and glass, which have higher refractive indexes than the aqueous media in which cells are immersed. The light is totally reflected according to Snell's law, but a small amount of energy passes through the interface into the lower refractive index media in the form of an evanescent wave that penetrates the specimen, typically 50–100 nm. Only the fluorescent molecules reached by the evanescent wave will be visible, enabling very selective, high-contrast fluorescence imaging. Recently, TIRFM has been used for single-molecule imaging because the background noise, which is a major problem during single-molecule imaging in an aqueous environment, can be overcome by limiting the illumination of excitation light to very near the glass surface. In this way, noise derived from Raman scattering of water molecules and out-of-focus fluorophores is dramatically reduced. The single-molecule imaging technique has already been applied successfully to a wide range of biological systems [67]. It is especially useful in studying the interaction between a ligand and a receptor on the cell surface, cell adhesion onto a surface [68], membrane dynamic or cellular secretion, electron transport in the mitochondrial membrane, cytoskeletal and membrane dynamics [69–73], cellular secretion events [74, 75], and ion transports [76, 77]. TIRF is also useful in studying the conformational dynamics of proteins or binding and triggering of cells by hormones.

Förster Resonance Energy Transfer (FRET)

Förster resonance energy transfer (FRET) is used to study inter- and intra-molecular interactions in living cells and is based on the transfer of non-radiative energy from a donor to an accepting fluorophore.

The resonance energy transfer process can occur when a fluorophore in its excited state, acting as a donor, transfers its excitation energy to an acceptor fluorophore. The transfer is due to a long-range dipole–dipole intermolecular coupling and is satisfied if the fluorescence emission spectrum of the donor overlaps that of the acceptor fluorophore, and the two probes are within a

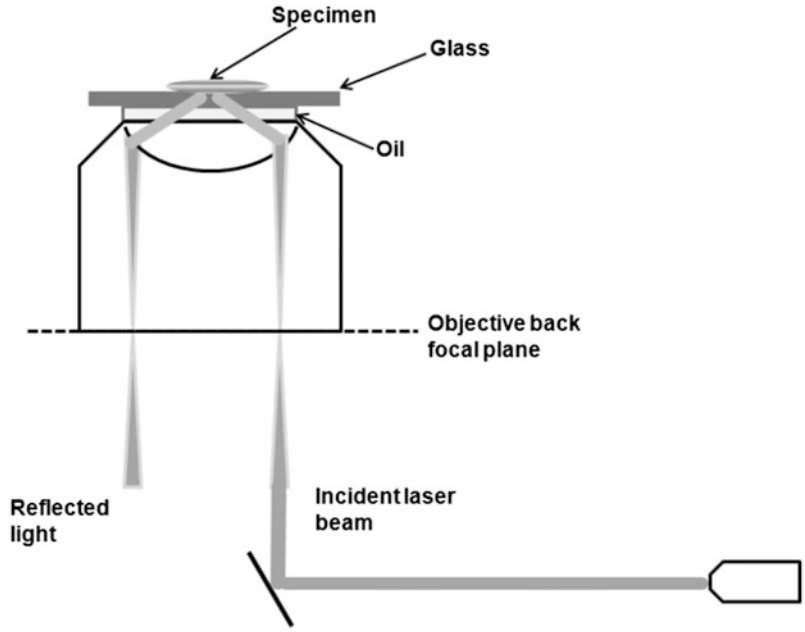

Fig. 4.5 Schematic picture of a total internal reflection fluorescence microscope

minimal spatial radius of 10 nm. In fact, according to the Förster equation, the transfer depends on the molecular distance at an inverse sixth power:

$$K_{\mathrm{T}} = (1/t_{\mathrm{D}}) \cdot [R_0/r]^6$$

where R_0 is the Förster critical distance, t_{D} is the donor lifetime in the absence of the acceptor, and r is the distance separating the donor and acceptor chromophores.

The Förster critical distance R_0 is defined as the acceptor–donor separation distance for which the transfer rate is equal to the rate of donor decay in the absence of an acceptor. This means that, at a Förster critical distance, 50 % of the donor excitation energy is transferred to the acceptor, whereas the remaining energy is dissipated through fluorescence emission or a thermal process [78, 79].

Besides studies of intermolecular and intramolecular mechanisms, FRET has also been used to explore structural and functional modifications in lipids and proteins. However, this technique requires the use of appropriate fluorophores to label specific targets in living cells; this problem has been overcome in some cases by cloning the jellyfish green fluorescent protein (GFP). GFP can be converted via site-directed mutagenesis into a blue fluorescent protein (BFP) [80]. GFP and BFP mutants possess the fluorescence characteristics to be employed in FRET experiments. Furthermore, FRET microscopy has been extended to the imaging of multiple donor–acceptor pairs by means of a three-fluorophore system using blue, yellow, and red fluorescent proteins [81]. Coupled with advances in pulsed lasers, microscope optics, and computer-based imaging technology, the development of labeling techniques in which the donor and acceptor fluorophores are actually part of the biomolecules themselves has enabled the visualization of dynamic protein interactions within living cells. In addition to the investigation of protein partner interactions, FRET has recently also been applied in studies of protease activity, alterations in membrane voltage potential, calcium metabolism, and the conduction of high-throughput screening assays, such as for quantification of gene expression in single living cells. FRET can also be used to study nucleic acid structural dynamics and the conformational diversity of nucleic acid structure hybridization

[82–84]. FRET is also used in a melting assay that allows the testing of libraries of compounds against different nucleic acid structures to determine whether they stabilize preformed structures [82].

Various examples of FRET use may be found in the scientific literature. Between 1997 and 1998, FRET was used to study Bax and BCL-2 interaction as well as their role in tumorigenesis and apoptosis.

More recently, FRET has been used to analyze the growth processes of axons, and thus the effects of sphingolipids on cerebrovascular permeability and the activation of macrophages by airway mucus. Therefore, FRET is still an effective way to investigate molecular interactions [81, 85–96]. Figure 1 provides an example of images and data gained by FRET.

Fluorescence Recovery After Photobleaching (FRAP)

Photobleaching is a photodynamic event and generally an unwanted phenomenon in fluorescence microscopy because it reduces the intensity of the probe fluorescence. Photobleaching involves the interaction of the fluorophore with a combination of light and oxygen after lengthy irradiation of molecules. The oxygen radical reacts with the more reactive excited fluorophore. The amount of photobleaching is a function of the molecular oxygen concentration and the distance between the fluorophore, oxygen molecules, and other cellular components. Reactions between fluorophores and molecular oxygen permanently destroy fluorescence, quenching light emission.

However, this quenching can be used in FRAP investigations to determine the kinetics of diffusion in living cells [97–103]. In fact, if a small portion of the cell is subjected to lengthy irradiation, the fluorescence in that area is completely quenched. The diffusion or active movement of molecules within the cell then replace the bleached fluorophore with unbleached molecules that were located in a different part of the cell and thus restore the fluorescence. By monitoring the intensity of the fluorescence emission, the translational mobility of a probe can be determined within a very small (2–5 μm) region of a single cell or section of living tissue.

Requirements for FRAP:

1. "Moving" objects must be labeled with a fluorophore.
2. Equipment must be able to bleach a defined area.

FRAP detects:

- Diffusion of molecules
- Active movement of cell components
- Recycling of cell components

The modern fluorescence microscope can provide more information, further enhanced by the informatics instruments that are now available. Digital images combined with FRAP enable the acquisition of information at low light levels or at visually undetectable wavelengths. These technical improvements are now an integral part of the techniques discussed here. Several years ago, optical microscopy was purely a descriptive instrument, whereas now it represents the first step of a more detailed pathway. The microscope accomplishes this first step in conjunction with electronic detectors, image processors, and display devices that can be viewed as extensions of the imaging system.

Technique Description and Examples

The basic function of a fluorescence microscope is to irradiate specimens with the right wavelength and separate the weaker emitted fluorescence from the excitation light. Only the emission light should reach the eye, or detector, leading to fluorescent structures being displayed as a high-contrast color on a very dark (or black) background. The limits of detection are generally related to the darkness of the background and the excitation light, which is typically from several hundred thousand to a million times brighter than the emitted fluorescence. Photobleaching is the irreversible

decomposition of the fluorescent molecules in the excited state because of their interaction with molecular oxygen before emission. Among very recent applications of the FRAP technique [104–110], we note investigations of chromatin mobility and structure [111, 112] and analysis of protozoan flagellar proteins [113].

Fluorescence Lifetime Imaging Microscopy (FLIM)

Fluorescence lifetime can be defined as the average time a molecule spends in its excited singlet state before spontaneous emission occurs. The fluorescence lifetime of a fluorophore can be described as the decrease in the number of excited fluorophores during the time following optical excitation with a very short light pulse. Generally, since the excited state of a fluorophore has a time interval between 1 and 20 ns, the excitation pulse must be about 100 ps to avoid excitation and emission coincident light. Fluorescence lifetime possesses some advantages over conventional fluorescence microscopy because each fluorescent dye has its own lifetime in the excited state. Thus, by detecting differences in lifetime, it is possible to distinguish dyes with overlapping fluorescent wavelengths or autofluorescence, which can be undistinguishable with conventional fluorescence microscopy based on spectral characteristics. In addition, fluorescence lifetime imaging microscopy (FLIM) finds its most significant applications in visualizing environmental changes of a probe in a living cell [97, 114]. As discussed previously, a fluorophore in the excited state possesses a higher dipolar moment that can be affected by solvent polarity changes due to ions, pH, and changes in its localization within the cell organelles or binding with other molecules [115–117]. Since the lifetime depends on the excited state, solvent change can change the lifetime of the fluorophore. In fact, the emission spectrum of the fluorophore also changes with solvent polarity; a maximum red shift is generally observed by increasing solvent polarity. However, this shift is generally smaller than the wavelength range of the band-pass emission filter. Furthermore, lifetime is independent of dye concentration, photobleaching, light scattering, and excitation light intensity; therefore, FLIM enables accurate ion concentration measurement and FRET analysis [118, 119].

Two methods of FLIM are used: the time–domain method and the frequency–domain method.

Frequency-Domain FLIM

In frequency–domain measurement, the sample is excited by a frequency sinusoidally modulated laser source (1–200 MHz). The phase and amplitude of the exciting light are measured; the lifetime of each fluorophore causes a unique phase shift and attenuation at a given frequency. The measurement may be taken either by a photomultiplier or using a CCD. However, this method, despite having a high temporal resolution, has limited ability to provide spatial information. Usually, FLIM instruments for frequency–domain methods are designed to operate at frequencies between 10 and 100 MHz, since most fluorochromes frequently used in biomedical research have lifetimes ranging from 1 to 10 ns [120].

Time–Domain FLIM

Time-resolved fluorescence takes advantage of high-speed pulsed lasers with picosecond pulses with fast recurrence rates and a high-speed gate image intensifier to acquire emitted photons. Emitted photons can be collected in two ways: time-correlated single photon counting (TCSPC) and the acquisition of a fixed number of photons (two to eight) in distinct time intervals using gated detection. In TCSPC, the elapsed time to reach the detector by the first photon after each pulse is monitored at a very high time resolution. A decay plot is obtained by recording the elapsed times of a large number of photons. In the other method, fluorescence intensity is monitored as a function of time by integrating the area under the

curve describing the exponential decay at two distinct time intervals after pulse.

Frequency–domain FLIM was used by Bastiaens et al. [121] to measure the average fluorescence lifetimes of six GFP variants, which were found to range in value from 1.3 to 3.7 ns. The ability to distinguish fusion proteins labeled with different GFP variants gives the chance to obtain information from different proteins simultaneously in a single experiment using multi-labeling imaging of live cells. Sabatini et al. [115] measured cyclic adenosine monophosphate (cAMP)-dependent protein kinase A (PKA) activity in brain tissue in FRET–FLIM experiments using an A-kinase activity reporter (AKAR).

References

1. Parrilla E, Armengot M, Mata M, Sanchez-Vilchez JM, Cortijo J, Hueso JL, Riera J, Moratal D. Primary ciliary dyskinesia assessment by means of optical flow analysis of phase-contrast microscopy images. Comput Med Imaging Graph. 2014;38:163–70.
2. Kong L, Doona CJ, Setlow P, Li YQ. Monitoring rates and heterogeneity of high-pressure germination of bacillus spores by phase-contrast microscopy of individual spores. Appl Environ Microbiol. 2014;80:345–53.
3. Jaccard N, Griffin LD, Keser A, Macown RJ, Super A, Veraitch FS, Szita N. Automated method for the rapid and precise estimation of adherent cell culture characteristics from phase contrast microscopy images. Biotechnol Bioeng. 2014;111:504–17.
4. Thirusittampalam K, Hossain MJ, Ghita O, Whelan PF. A novel framework for cellular tracking and mitosis detection in dense phase contrast microscopy images. IEEE J Biomed Health Inform. 2013;17:642–53.
5. Steiger R, Bernet S, Ritsch-Marte M. Mapping of phase singularities with spiral phase contrast microscopy. Opt Express. 2013;21:16282–9.
6. Su H, Yin Z, Huh S, Kanade T. Cell segmentation in phase contrast microscopy images via semi-supervised classification over optics-related features. Med Image Anal. 2013;17:746–65.
7. Kong Z, Zhu X, Zhang S, Wu J, Luo Y. Phase contrast microscopy of living cells within the whole lens: spatial correlations and morphological dynamics. Mol Vis. 2012;18:2165–73.
8. Nejati Javaremi A, Unsworth CP, Graham ES. A cell derived active contour (CDAC) method for robust tracking in low frame rate, low contrast phase microscopy—an example: the human hNT astrocyte. PLoS One. 2013;8:e82883.
9. Rigaud S, Huang CH, Ahmed S, Lim JH, Racoceanu D. An analysis-synthesis approach for neurosphere modelisation under phase-contrast microscopy. Conf Proc IEEE Eng Med Biol Soc. 2013;2013:3989–92.
10. Liu A, Hao T, Gao Z, Su Y, Yang Z. Nonnegative mixed-norm convex optimization for mitotic cell detection in phase contrast microscopy. Comput Math Methods Med. 2013;2013:176272.
11. Huh S, Kanade T. Apoptosis detection for non-adherent cells in time-lapse phase contrast microscopy. Med Image Comput Comput Assist Interv. 2013;16:59–66.
12. Hooley EN, Tilley AJ, White JM, Ghiggino KP, Bell TD. Energy transfer in PPV-based conjugated polymers: a defocused widefield fluorescence microscopy study. Phys Chem Chem Phys. 2014;16:7108–14.
13. Juneau PM, Garnier A, Duchesne C. Selection and tuning of a fast and simple phase-contrast microscopy image segmentation algorithm for measuring myoblast growth kinetics in an automated manner. Microsc Microanal. 2013;19:855–66.
14. Huh S, Su H, Chen M, Kanade T. Efficient phase contrast microscopy restoration applied for muscle myotube detection. Med Image Comput Comput Assist Interv. 2013;16:420–7.
15. Kim J, An S, Ahn S, Kim B. Depth-variant deconvolution of 3D widefield fluorescence microscopy using the penalized maximum likelihood estimation method. Opt Express. 2013;21:27668–81.
16. Yin Z, Kanade T, Chen M. Understanding the phase contrast optics to restore artifact-free microscopy images for segmentation. Med Image Anal. 2012;16:1047–62.
17. Piper T, Piper J. Axial phase-darkfield-contrast (APDC), a new technique for variable optical contrasting in light microscopy. J Microsc. 2012;247:259–68.
18. Chatterjee S, Pavan Kumar Y. White light differential interference contrast microscope with a Sagnac interferometer. Appl Optics. 2014;53:296–300.
19. Chen J, Xu Y, Lv X, Lai X, Zeng S. Super-resolution differential interference contrast microscopy by structured illumination. Opt Express. 2013;21:112–21.
20. Chen J, Lv X, Zeng S. Doubling the resolution of spatial-light-modulator-based differential interference contrast microscopy by structured illumination. Opt Lett. 2013;38:3219–22.
21. Battle C, Lautscham L, Schmidt CF. Differential interference contrast microscopy using light-emitting diode illumination in conjunction with dual optical traps. Rev Sci Instrum. 2013;84:053703.
22. Kim M, Choi Y, Fang-Yen C, Sung Y, Kim K, Dasari RR, Feld MS, Choi W. Three-dimensional differential interference contrast microscopy using synthetic aperture imaging. J Biomed Opt. 2012;17:026003.
23. Luo Y, Sun W, Gu Y, Wang G, Fang N. Wavelength-dependent differential interference contrast microscopy: multiplexing detection using nonfluorescent nanoparticles. Anal Chem. 2010;82:6675–9.

24. Zhu Y, Shaked NT, Satterwhite LL, Wax A. Spectral-domain differential interference contrast microscopy. Opt Lett. 2011;36:430–2.
25. McIntyre TJ, Maurer C, Bernet S, Ritsch-Marte M. Differential interference contrast imaging using a spatial light modulator. Opt Lett. 2009;34:2988–90.
26. Yang X, Qin L, Liang W, Wang W, Tan J, Liang P, Xu J, Li S, Cui S. New bone formation and microstructure assessed by combination of confocal laser scanning microscopy and differential interference contrast microscopy. Calcif Tissue Int. 2014;94:338–47.
27. Oh J, Kim SH, Kim YJ, Lee H, Cho JH, Cho YH, Kim CK, Lee TJ, Lee S, Park KH, Yu HG, Lee HJ, Jun SC, Kim JH. Detection of retinitis pigmentosa by differential interference contrast microscopy. PLoS One. 2014;9:e97170.
28. McPhee CI, Zoriniants G, Langbein W, Borri P. Measuring the lamellarity of giant lipid vesicles with differential interference contrast microscopy. Biophys J. 2013;105:1414–20.
29. Baker-Groberg SM, Phillips KG, McCarty OJ. Quantification of volume, mass, and density of thrombus formation using brightfield and differential interference contrast microscopy. J Biomed Opt. 2013;18:16014.
30. Tsunoda M, Isailovic D, Yeung ES. Real-time three-dimensional imaging of cell division by differential interference contrast microscopy. J Microsc. 2008;232:207–11.
31. Yenjerla M, Lopus M, Wilson L. Analysis of dynamic instability of steady-state microtubules in vitro by video-enhanced differential interference contrast microscopy with an appendix by Emin Oroudjev. Methods Cell Biol. 2010;95:189–206.
32. Wolf DE. Fundamentals of fluorescence and fluorescence microscopy. Methods Cell Biol. 2013;114:69–97.
33. Webb DJ, Brown CM. Epi-fluorescence microscopy. Methods Mol Biol. 2013;931:29–59.
34. Renz M. Fluorescence microscopy-a historical and technical perspective. Cytometry A. 2013;83:767–79.
35. Basic Concepts in Fluorescence. http://micro.magnet.fsu.edu/primer/techniques/fluorescence/fluorescenceintro.html
36. Fritzky L, Lagunoff D. Advanced methods in fluorescence microscopy. Anal Cell Pathol. 2013;36:5–17.
37. Luo W, He K, Xia T, Fang X. Single-molecule monitoring in living cells by use of fluorescence microscopy. Anal Bioanal Chem. 2013;405:43–9.
38. Tahir M, Khan A, Kaya H. Protein subcellular localization in human and hamster cell lines: employing local ternary patterns of fluorescence microscopy images. J Theor Biol. 2014;340:85–95.
39. Duheron V, Moreau M, Collin B, Sali W, Bernhard C, Goze C, Gautier T, Pais de Barros JP, Deckert V, Brunotte F, Lagrost L, Denat F. Dual labeling of lipopolysaccharides for SPECT-CT imaging and fluorescence microscopy. ACS Chem Biol. 2014;9:656–62.
40. Ujihara Y, Nakamura M, Miyazaki H, Wada S. Segmentation and morphometric analysis of cells from fluorescence microscopy images of cytoskeletons. Comput Math Methods Med. 2013;2013:381356.
41. Tapley A, Switz N, Reber C, Davis JL, Miller C, Matovu JB, Worodria W, Huang L, Fletcher DA, Cattamanchi A. Mobile digital fluorescence microscopy for diagnosis of tuberculosis. J Clin Microbiol. 2013;51:1774–8.
42. Scholz D, Fortsch J, Bockler S, Klecker T, Westermann B. Analyzing membrane dynamics with live cell fluorescence microscopy with a focus on yeast mitochondria. Methods Mol Biol. 2013;1033:275–83.
43. Yan Y, Petchprayoon C, Mao S, Marriott G. Reversible optical control of cyanine fluorescence in fixed and living cells: optical lock-in detection immunofluorescence imaging microscopy. Philos Trans R Soc Lond B Biol Sci. 2013;368:20120031.
44. Furia L, Pelicci PG, Faretta M. A computational platform for robotized fluorescence microscopy (I): high-content image-based cell-cycle analysis. Cytometry A. 2013;83:333–43.
45. Furia L, Pelicci PG, Faretta M. A computational platform for robotized fluorescence microscopy (II): DNA damage, replication, checkpoint activation, and cell cycle progression by high-content high-resolution multiparameter image-cytometry. Cytometry A. 2013;83:344–55.
46. Laser Scanning Confocal Microscopy. http://micro.magnet.fsu.edu/primer/techniques/confocal/index.html
47. Ragazzi M, Piana S, Longo C, Castagnetti F, Foroni M, Ferrari G, Gardini G, Pellacani G. Fluorescence confocal microscopy for pathologists. Mod Pathol. 2014;27:460–71.
48. Herberich G, Windoffer R, Leube RE, Aach T. Signal and noise modeling in confocal laser scanning fluorescence microscopy. Med Image Comput Comput Assist Interv. 2012;15:381–8.
49. Wu Y, Zinchuk V, Grossenbacher-Zinchuk O, Stefani E. Critical evaluation of quantitative colocalization analysis in confocal fluorescence microscopy. Interdiscip Sci. 2012;4:27–37.
50. Balestrieri ML, Giovane A, Milone L, Servillo L. Endothelial progenitor cells express PAF receptor and respond to PAF via Ca(2+)-dependent signaling. Biochim Biophys Acta. 2010;1801:1123–32.
51. Coxon FP. Fluorescence imaging of osteoclasts using confocal microscopy. Methods Mol Biol. 2012;816:401–24.
52. Kress A, Wang X, Ranchon H, Savatier J, Rigneault H, Ferrand P, Brasselet S. Mapping the local organization of cell membranes using excitation-polarization-resolved confocal fluorescence microscopy. Biophys J. 2013;105:127–36.
53. Feola A, Cimini A, Migliucci F, Iorio R, Zuchegna C, Rothenberger R, Cito L, Porcellini A, Unteregger G, Tombolini V, Giordano A, Di Domenico M. The inhibition of p85alphaPI3KSer83 phosphorylation prevents cell proliferation and invasion in prostate cancer cells. J Cell Biochem. 2013;114:2114–9.

54. Cosentino C, Di Domenico M, Porcellini A, Cuozzo C, De Gregorio G, Santillo MR, Agnese S, Di Stasio R, Feliciello A, Migliaccio A, Avvedimento EV. p85 regulatory subunit of PI3K mediates cAMP-PKA and estrogens biological effects on growth and survival. Oncogene. 2007;26:2095–103.
55. Longo C, Rajadhyaksha M, Ragazzi M, Nehal K, Gardini S, Moscarella E, Lallas A, Zalaudek I, Piana S, Argenziano G, Pellacani G. Evaluating ex vivo fluorescence confocal microscopy images of basal cell carcinomas in Mohs excised tissue. Br J Dermatol. 2014;171(3):561–70.
56. Dobbs JL, Ding H, Benveniste AP, Kuerer HM, Krishnamurthy S, Yang W, Richards-Kortum R. Feasibility of confocal fluorescence microscopy for real-time evaluation of neoplasia in fresh human breast tissue. J Biomed Opt. 2013;18:106016.
57. Bennassar A, Carrera C, Puig S, Vilalta A, Malvehy J. Fast evaluation of 69 basal cell carcinomas with ex vivo fluorescence confocal microscopy: criteria description, histopathological correlation, and inter-observer agreement. JAMA Dermatol. 2013;149:839–47.
58. De Gregorio G, Coppa A, Cosentino C, et al. The p85 regulatory subunit of PI3K mediates TSHcAMP-PKA growth and survival signals. Oncogene. 2007;26:2039–47.
59. Altomare DA, Testa JR. Perturbations of the AKT signaling pathway in human cancer. Oncogene. 2005;24:7455–64.
60. Vega FM, Fruhwirth G, Ng T, Ridley AJ. RhoA and RhoC have distinct roles in migration and invasion by acting through different targets. J Cell Biol. 2011;193:655–64.
61. Total Internal Reflection Fluorescence Microscopy. http://micro.magnet.fsu.edu/primer/techniques/fluorescence/tirf/tirfhome.html
62. Brunstein M, Teremetz M, Herault K, Tourain C, Oheim M. Eliminating unwanted far-field excitation in objective-type TIRF. Part I. Identifying sources of nonevanescent excitation light. Biophys J. 2014;106:1020–32.
63. Brunstein M, Herault K, Oheim M. Eliminating unwanted far-field excitation in objective-type TIRF. Part II. Combined evanescent-wave excitation and supercritical-angle fluorescence detection improves optical sectioning. Biophys J. 2014;106:1044–56.
64. Lane RS, Macpherson AN, Magennis SW. Signal enhancement in multiphoton TIRF microscopy by shaping of broadband femtosecond pulses. Opt Express. 2012;20:25948–59.
65. Johnson DS, Jaiswal JK, Simon S. Total internal reflection fluorescence (TIRF) microscopy illuminator for improved imaging of cell surface events. Curr Protoc Cytom. 2012;Chapter 12, Unit 12 29.
66. Liang L, Shen H, De Camilli P, Toomre DK, Duncan JS. An expectation maximization based method for subcellular particle tracking using multi-angle TIRF microscopy. Med Image Comput Comput Assist Interv. 2011;14:629–36.
67. Oheim M. Quantitative imaging of single-organelle and single-molecule dynamics near the plasma membrane using a combination of spinning TIRF and virtual supercritical-angle detection. Biomed Tech. 2012. doi:10.1515/bmt-2012-4565.
68. Charlton C, Gubala V, Gandhiraman RP, Wiechecki J, Le NC, Coyle C, Daniels S, Maccraith BD, Williams DE. TIRF microscopy as a screening method for non-specific binding on surfaces. J Colloid Interface Sci. 2011;354:405–9.
69. Parhamifar L, Moghimi SM. Total internal reflection fluorescence (TIRF) microscopy for real-time imaging of nanoparticle-cell plasma membrane interaction. Methods Mol Biol. 2012;906:473–82.
70. Loder MK, Tsuboi T, Rutter GA. Live-cell imaging of vesicle trafficking and divalent metal ions by total internal reflection fluorescence (TIRF) microscopy. Methods Mol Biol. 2013;950:13–26.
71. Leslie K, Galjart N. Going solo: measuring the motions of microtubules with an in vitro assay for TIRF microscopy. Methods Cell Biol. 2013;115:109–24.
72. Telley IA, Bieling P, Surrey T. Reconstitution and quantification of dynamic microtubule end tracking in vitro using TIRF microscopy. Methods Mol Biol. 2011;777:127–45.
73. Ross JA, Digman MA, Wang L, Gratton E, Albanesi JP, Jameson DM. Oligomerization state of dynamin 2 in cell membranes using TIRF and number and brightness analysis. Biophys J. 2011;100:L15–7.
74. Matz M, Schumacher K, Hatlapatka K, Lorenz D, Baumann K, Rustenbeck I. Observer-independent quantification of insulin granule exocytosis and pre-exocytotic mobility by TIRF microscopy. Microsc Microanal. 2014;20:206–18.
75. Akopova I, Tatur S, Grygorczyk M, Luchowski R, Gryczynski I, Gryczynski Z, Borejdo J, Grygorczyk R. Imaging exocytosis of ATP-containing vesicles with TIRF microscopy in lung epithelial A549 cells. Purinergic Signal. 2012;8:59–70.
76. Sidaway P, Teramoto N. L-type Ca^{2+} channel sparklets revealed by TIRF microscopy in mouse urinary bladder smooth muscle. PLoS One. 2014;9:e93803.
77. Ramachandran S, Arce FT, Patel NR, Quist AP, Cohen DA, Lal R. Structure and permeability of ion-channels by integrated AFM and waveguide TIRF microscopy. Sci Rep. 2014;4:4424.
78. Pietraszewska-Bogiel A, Gadella TW. FRET microscopy: from principle to routine technology in cell biology. J Microsc. 2011;241:111–8.
79. Sun Y, Wallrabe H, Seo SA, Periasamy A. FRET microscopy in 2010: the legacy of Theodor Forster on the 100th anniversary of his birth. Chemphyschem. 2011;12:462–74.
80. Giron MD, Salto R. From green to blue: site-directed mutagenesis of the green fluorescent protein to teach protein structure-function relationships. Biochem Mol Biol Educ. 2011;39:309–15.
81. Hoppe AD, Scott BL, Welliver TP, Straight SW, Swanson JA. N-way FRET microscopy of multiple

protein-protein interactions in live cells. PLoS One. 2013;8:e64760.
82. Kruger AC, Birkedal V. Single molecule FRET data analysis procedures for FRET efficiency determination: probing the conformations of nucleic acid structures. Methods. 2013;64:36–42.
83. Simkova E, Stanek D. Probing nucleic acid interactions and Pre-mRNA splicing by Forster resonance energy transfer (FRET) microscopy. Int J Mol Sci. 2012;13:14929–45.
84. Renciuk D, Zhou J, Beaurepaire L, Guedin A, Bourdoncle A, Mergny JL. A FRET-based screening assay for nucleic acid ligands. Methods. 2012;57:122–8.
85. Guo Q, He Y, Lu HP. Manipulating and probing enzymatic conformational fluctuations and enzyme-substrate interactions by single-molecule FRET-magnetic tweezers microscopy. Phys Chem Chem Phys. 2014;16(26):13052–8.
86. Canclini L, Wallrabe H, Di Paolo A, Kun A, Calliari A, Sotelo-Silveira JR, Sotelo JR. Association of Myosin Va and Schwann cells-derived RNA in mammal myelinated axons, analyzed by immunocytochemistry and confocal FRET microscopy. Methods. 2014;66:153–61.
87. Ziomkiewicz I, Loman A, Klement R, Fritsch C, Klymchenko AS, Bunt G, Jovin TM, Arndt-Jovin DJ. Dynamic conformational transitions of the EGF receptor in living mammalian cells determined by FRET and fluorescence lifetime imaging microscopy. Cytometry A. 2013;83:794–805.
88. Wallrabe H, Cai Y, Sun Y, Periasamy A, Luzes R, Fang X, Kan HM, Cameron LC, Schafer DA, Bloom GS. IQGAP1 interactome analysis by in vitro reconstitution and live cell 3-color FRET microscopy. Cytoskeleton. 2013;70:819–36.
89. Prasad S, Zeug A, Ponimaskin E. Analysis of receptor-receptor interaction by combined application of FRET and microscopy. Methods Cell Biol. 2013;117:243–65.
90. Grecco HE, Bastiaens PI. Quantifying cellular dynamics by fluorescence resonance energy transfer (FRET) microscopy. Curr Protoc Neurosci. 2013; Chapter 5, Unit 5 22.
91. Sprenger JU, Perera RK, Gotz KR, Nikolaev VO. FRET microscopy for real-time monitoring of signaling events in live cells using unimolecular biosensors. J Vis Exp. 2012;e4081.
92. Roberts SK, Tynan CJ, Winn M, Martin-Fernandez ML. Investigating extracellular in situ EGFR structure and conformational changes using FRET microscopy. Biochem Soc Trans. 2012;40:189–94.
93. Padilla-Parra S, Tramier M. FRET microscopy in the living cell: different approaches, strengths and weaknesses. Bioessays. 2012;34:369–76.
94. Ferrari ML, Gomez GA, Maccioni HJ. Spatial organization and stoichiometry of N-terminal domain-mediated glycosyltransferase complexes in Golgi membranes determined by fret microscopy. Neurochem Res. 2012;37:1325–34.
95. Day RN, Davidson MW. Fluorescent proteins for FRET microscopy: monitoring protein interactions in living cells. Bioessays. 2012;34:341–50.
96. Goncalves JT, Stuhmer W. Calmodulin interaction with hEAG1 visualized by FRET microscopy. PLoS One. 2010;5:e10873.
97. Ishikawa-Ankerhold HC, Ankerhold R, Drummen GP. Advanced fluorescence microscopy techniques–FRAP, FLIP, FLAP, FRET and FLIM. Molecules. 2012;17:4047–132.
98. Yang J, Kohler K, Davis DM, Burroughs NJ. An improved strip FRAP method for estimating diffusion coefficients: correcting for the degree of photobleaching. J Microsc. 2010;238:240–53.
99. Kang M, Day CA, DiBenedetto E, Kenworthy AK. A quantitative approach to analyze binding diffusion kinetics by confocal FRAP. Biophys J. 2010;99:2737–47.
100. Kang M, Day CA, Kenworthy AK, DiBenedetto E. Simplified equation to extract diffusion coefficients from confocal FRAP data. Traffic. 2012;13:1589–600.
101. Xiong R, Deschout H, Demeester J, De Smedt SC, Braeckmans K. Rectangle FRAP for measuring diffusion with a laser scanning microscope. Methods Mol Biol. 2014;1076:433–41.
102. Wachsmuth M. Molecular diffusion and binding analyzed with FRAP. Protoplasma. 2014;251:373–82.
103. Deschout H, Raemdonck K, Demeester J, De Smedt SC, Braeckmans K. FRAP in pharmaceutical research: practical guidelines and applications in drug delivery. Pharm Res. 2014;31:255–70.
104. Groeneweg FL, van Royen ME, Fenz S, Keizer VI, Geverts B, Prins J, de Kloet ER, Houtsmuller AB, Schmidt TS, Schaaf MJ. Quantitation of glucocorticoid receptor DNA-binding dynamics by single-molecule microscopy and FRAP. PLoS One. 2014;9:e90532.
105. Watanabe N, Yamashiro S, Vavylonis D, Kiuchi T. Molecular viewing of actin polymerizing actions and beyond: combination analysis of single-molecule speckle microscopy with modeling, FRAP and s-FDAP (sequential fluorescence decay after photoactivation). Dev Growth Differ. 2013;55:508–14.
106. Schneider K, Fuchs C, Dobay A, Rottach A, Qin W, Wolf P, Alvarez-Castro JM, Nalaskowski MM, Kremmer E, Schmid V, Leonhardt H, Schermelleh L. Dissection of cell cycle-dependent dynamics of Dnmt1 by FRAP and diffusion-coupled modeling. Nucleic Acids Res. 2013;41:4860–76.
107. Bougault C, Cueru L, Bariller J, Malbouyres M, Paumier A, Aszodi A, Berthier Y, Mallein-Gerin F, Trunfio-Sfarghiu AM. Alteration of cartilage mechanical properties in absence of beta1 integrins revealed by rheometry and FRAP analyses. J Biomech. 2013;46:1633–40.

108. Hardy LR. Fluorescence recovery after photobleaching (FRAP) with a focus on F-actin. Curr Protoc Neurosci. 2012;Chapter 2, Unit 2 17.
109. Day CA, Kraft LJ, Kang M, Kenworthy AK. Analysis of protein and lipid dynamics using confocal fluorescence recovery after photobleaching (FRAP). Curr Protoc Cytom. 2012;Chapter 2, Unit 2 19.
110. Aguila B, Simaan M, Laporte SA. Study of G protein-coupled receptor/beta-arrestin interactions within endosomes using FRAP. Methods Mol Biol. 2011;756:371–80.
111. Bošković A, Eid A, Pontabry J, Ishiuchi T, Spiegelhalter C, Raghu Ram EV, Meshorer E, Torres-Padilla ME. Higher chromatin mobility supports totipotency and precedes pluripotency in vivo. Genes Dev. 2014;28(10):1042–7.
112. Bernas T, Brutkowski W, Zarębski M, Dobrucki J. Spatial heterogeneity of dynamics of H1 linker histone. Eur Biophys J. 2014;43:287–300.
113. Subota I, Julkowska D, Vincensini L, Reeg N, Buisson J, Blisnick T, Huet D, Perrot S, Santi-Rocca J, Duchateau M, Hourdel V, Rousselle JC, Cayet N, Namane A, Chamot-Rooke J, Bastin P. Proteomic analysis of intact flagella of procyclic Trypanosoma brucei cells identifies novel flagellar proteins with unique sub-localisation and dynamics. Mol Cell Proteomics. 2014;13(7):1769–86.
114. Pande P, Jo JA. Automated analysis of fluorescence lifetime imaging microscopy (FLIM) data based on the Laguerre deconvolution method. IEEE Trans BioMed Eng. 2011;58:172–81.
115. Chen Y, Saulnier JL, Yellen G, Sabatini BL. A PKA activity sensor for quantitative analysis of endogenous GPCR signaling via 2-photon FRET-FLIM imaging. Front Pharmacol. 2014;5:56.
116. Schmitt FJ, Thaa B, Junghans C, Vitali M, Veit M, Friedrich T. eGFP-pHsens as a highly sensitive fluorophore for cellular pH determination by fluorescence lifetime imaging microscopy (FLIM). Biochim Biophys Acta. 2014.
117. Paredes JM, Giron MD, Ruedas-Rama MJ, Orte A, Crovetto L, Talavera EM, Salto R, Alvarez-Pez JM. Real-time phosphate sensing in living cells using fluorescence lifetime imaging microscopy (FLIM). J Phys Chem B. 2013;117:8143–9.
118. Morton PE, Parsons M. Measuring FRET using time-resolved FLIM. Methods Mol Biol. 2011;769:403–13.
119. Oliveira AF, Yasuda R. An improved Ras sensor for highly sensitive and quantitative FRET-FLIM imaging. PloS one. 2013;8:e52874.
120. Schuermann KC, Grecco HE. flatFLIM: enhancing the dynamic range of frequency domain FLIM. Opt Express. 2012;20:20730–41.
121. Pepperkok R, Squire A, Geley S, Bastiaens PI. Simultaneous detection of multiple green fluorescent proteins in live cells by fluorescence lifetime imaging microscopy. Curr Biol. 1999;9:269–72.